

Deciphering the origin of spin current in spintronic terahertz emitters and its imprint on their electromagnetic radiation via time-dependent density functional theory

Ali Kefayati,¹ Yafei Ren,¹ M. Benjamin Jungfleisch,¹ Lars Gundlach,^{1,2} John Q. Xiao,¹ and Branislav K. Nikolić^{1,*}

¹*Department of Physics and Astronomy, University of Delaware, Newark, DE 19716, USA*

²*Department of Chemistry and Biochemistry, University of Delaware, Newark, DE 19716, USA*

Spin current flowing between femtosecond laser pulse (fsLP)-driven ferromagnetic metal and adjacent normal metal (NM) hosting strong spin-orbit coupling is invariably invoked to explain THz radiation believed to be emitted solely by NM layer. Despite being such a central concept, the microscopic origin of such interlayer spin current remains vague. It is also unclear if it directly imprints its time-dependence onto emitted THz radiation because far-field radiation can only be emitted by time-dependent charge current where a potentially large number of complex spin-to-charge conversion mechanisms can obscure direct relation between interlayer spin current and converted charge current within NM layer. Here, we employ recently developed [A. Kefayati *et al.*, Phys. Rev. Lett. **133**, 136704 (2024)] time-dependent density functional theory plus Jefimenko equations approach to extract spin current between Co and NM=Pt or W layer where Co is driven by fsLP responsible for its demagnetization, i.e., shrinking of its magnetization vector, $M^y(t)/M^y(t=0) < 1$ [while $M^x(t) \approx M^z(t) \approx 0$]. By comparing time dependence of spin current with those of other relevant quantities, we find that: (i) spin current is generated by demagnetization dynamics because it follows closely dM^y/dt , thus it is an example of quantum pumping phenomenon that cannot be captured by phenomenological notions (such as “spin voltage”) or semiclassical theories; (ii) time dependence of pumped spin current *does not follow* closely that of charge current emerging within NM layer via spin-to-charge conversion mechanisms; (iii) emitted THz radiation is dominated by charge current (i.e., its time derivative entering the Jefimenko equations) within Co layer, rather than usually assumed charge current [from (ii)] within NM layer, especially in the case of NM=W where spin-to-charge conversion by the inverse spin Hall effect is suppressed, despite large spin Hall angle of W, due to localization of excited electrons onto the outer unfilled d -orbitals of W.

The spin current flowing from femtosecond laser pulse (fsLP)-driven ferromagnetic metal (FM) layer toward adjacent normal metal (NM) within FM/NM bilayers is one of the central concept [1–5] in the field of ultrafast magnetism [6–8]. It is believed that such current (along the z -axis in Fig. 1) is converted into charge current (along the x -axis in Fig. 1) via either the inverse spin Hall effect (ISHE) [9] in the bulk of NM layer or other spin-orbit coupling (SOC)-driven mechanisms at FM/NM interfaces [10–12] due to the strong SOC in NM layer that is usually heavy transition metals (such as Pt, W, and Ta). It is, therefore, believed [13] that optimizing interlayer spin current and spin-to-charge conversion mechanisms can enhance THz radiation by enhancing spin-to-charge converted charge current I_{NM}^x (as denoted in Fig. 1) flowing within the NM layer.

However, the microscopic origin of interlayer spin current vector ($I_{S_\alpha}^x(t), I_{S_\alpha}^y(t), I_{S_\alpha}^z(t)$) [Fig. 1] remains unknown. Instead, interpretation of experiments is phenomenological and relies on intuitive notions of spin voltage or spin accumulation (a difference between nonequilibrium chemical potentials of the two spin species) [2, 4, 14], which then drives spin current according to semiclassical transport theories [15–17]. This picture does not explain features in the THz range contained in the frequency spectrum of spin-to-charge converted current [1] or the role played by demagnetization dynamics because spin voltage can be nonzero due to fsLP and magnetism within FM layer even if its magnetization is not

changing (as is the case if its SOC is artificially turned off [18, 19]). Furthermore, another standard picture [1–5] is that charge current $I_{\text{NM}}^x(t)$ flowing within NM layer, after spin-to-charge conversion takes place, is simply given by

$$I_{\text{NM}}^x(t) \equiv \theta_{\text{SH}} I_{S_y}^z(t), \quad (1)$$

where θ_{SH} is the spin Hall angle [20]. This equation, as well as the assumption that $I_{\text{NM}}^x(t)$ is the sole source of outgoing THz signal observed in the far-field (FF) region, forms then the basis for the time-domain THz emission spectroscopy study [5] where one assumes that spatial and temporal evolution of ultrafast spin currents, triggered by fsLP excitation of thin FM films, can be directly extracted from the time profile of measured THz signal. However, this might not be warranted as recent experiments [21] point to a potentially large number of complex spin-to-charge conversion mechanisms and high sensitivity to changes in the optical properties, as well as charge density equilibration [22], which can obscure one-to-one correspondence encoded by Eq. (1).

In this Letter, we employ time-dependent density functional theory [23, 24] (TDDFT)—which has provided most detailed microscopic insights [18, 25–27] into demagnetization mechanisms, and which has recently been extended [28] into TDDFT+Jefimenko approach for computation of currents and the ensuing electromagnetic (EM) radiation—to analyze fsLP-driven Co/Pt and Co/W bilayers. This approach allows us to extract, from

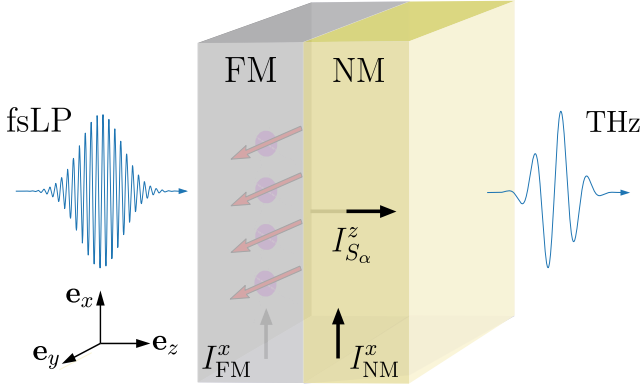


FIG. 1. Schematic view of FM/NM bilayer employed [1–4] for spintronic THz emitters where fsLP irradiates FM layer, such as Co we choose, and NM layer hosts strong SOC, such as Pt or W we choose for comparison with each other as their spin Hall angle has opposite sign [2]. The thickness of Co layer is three monolayers, while the thickness of NM layers is four monolayers. The local magnetization (red arrows) of Co layer is along the y -axis in equilibrium, and it remains so (i.e., $M^x \approx M^z \approx 0$) during demagnetization in nonequilibrium while only *shrinking* its length. Total spin current from FM to NM layer is denoted by $I_{S_{\alpha}}^z$ and total charge currents within FM or NM layers are denoted by I_{FM}^x and I_{NM}^x , respectively.

first principles, time-dependencies of: spin current from Co toward Pt or W layer [Fig. 2]; charge current flowing within Pt or W layer [Figs. 3(b,c)]; demagnetization dynamics $M^y(t)/M^y(t=0) < 1$ [while $M^x(t) \approx M^z(t) \approx 0$] within Co layer [Fig. 2]; and electric field $E_{FF}^x(t)$ of the emitted THz radiation in the far-field region [Figs. 3(c,f)]. Furthermore, it also makes it possible to analyze how total real-time THz signal from FM/NM bilayer emerges from contributions generated by FM (virtually never considered when analyzing experiments [1–5]) vs. NM layer (the only one considered when analyzing experiments thus far [1–5]), which does not have to be simple enhancement of each other as these two contributions could have different shape or phase [Fig. 3].

We commence by examining in Fig. 2 the possible causal connection between $\partial_t M^y$ (we use $\partial_t \equiv \partial/\partial t$) and interlayer spin current

$$I_{S_{\alpha}}^z(t) = \int_{\text{FM/NM}} d^3 r j_{S_{\alpha}}^z(\mathbf{r}, t), \quad (2)$$

transporting spins S_{α} along the z -axis [see coordinate system in Fig. 1], which is obtained by integrating one component $j_{S_{\alpha}}^z(\mathbf{r}, t)$ of 3×3 spin current density tensor [29] over the whole FM/NM bilayer. Note that we use the same units for spin and charge current, where spin current $I_{S_y}^z = I_z^{\uparrow} - I_z^{\downarrow}$ can be understood as the difference of the respective spin-resolved charge currents, I_z^{\uparrow} and I_z^{\downarrow} , with \uparrow, \downarrow pointing along the y -axis. The overlapping time-dependencies of $I_{S_y}^z(t)$ and $\partial_t M^y$ demon-

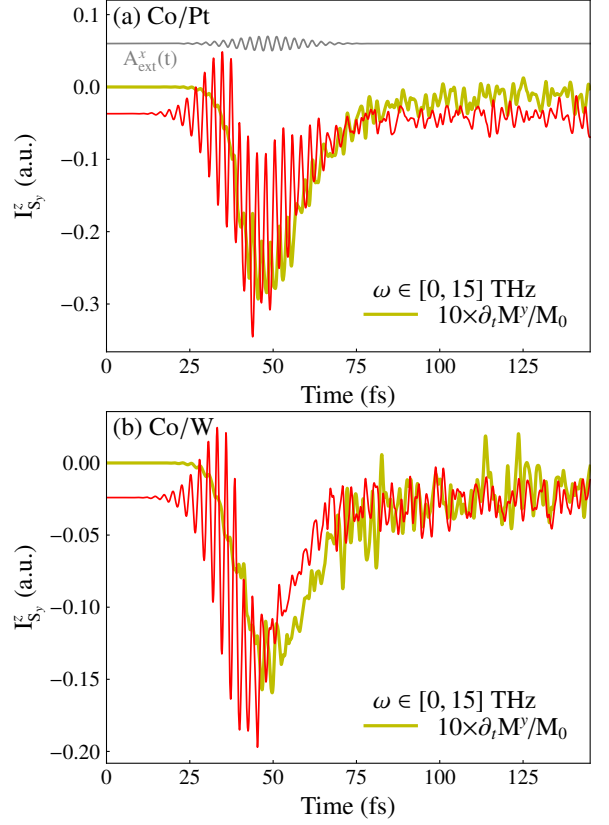


FIG. 2. Time-dependence of interlayer spin current $I_{S_y}^z$ (red curves) in fsLP-driven (a) Co/Pt and (b) Co/W bilayers is compared with that of time derivative of magnetization $\partial_t M^y/M_0$ (yellow curves), demonstrating a causal connection where the latter generates (or pumps) the former. Both panels are obtained by using Fourier components within $\omega \in [0, 15]$ THz range to reconstruct respective real time signals. We use $M_0 \equiv M^y(t=0)$ for magnetization in equilibrium pointing along the y -axis in Fig. 1. Gray curve in (a) depicts vector potential $A_{\text{ext}}^x(t)$ of fsLP in Eq. (5).

strate that dM^y/dt is the mechanisms behind spin current generation. This is akin to spin current pumping [30], where $(I_{S_x}, I_{S_y}, I_{S_z}) \propto \mathbf{M} \times \partial_t \mathbf{M}$, by time-dependent magnetization of fixed length which precesses at much smaller (typically GHz) single frequency when microwaves are absorbed under the ferromagnetic resonance conditions [9, 31]. In contrast to the precession of magnetization driven by low-frequency EM radiation, the shrinking of magnetization length due to fsLP drive, as well as $\partial_t M^y(t)$, contain [27] a continuum of much higher frequencies in its fast-Fourier transform. Nevertheless, in both “high-frequency” and “low-frequency” phenomena involving $\mathbf{M}(t)$, it is thereby induced time-dependence of the quantum systems [32, 33], periodic [30, 32–34] in the case of magnetization precession and non-periodic [35] in the case of the demagnetization, that pumps currents in the absence of any bias voltage. Thus, pumping of spin current by demagnetization dynamics unveiled by

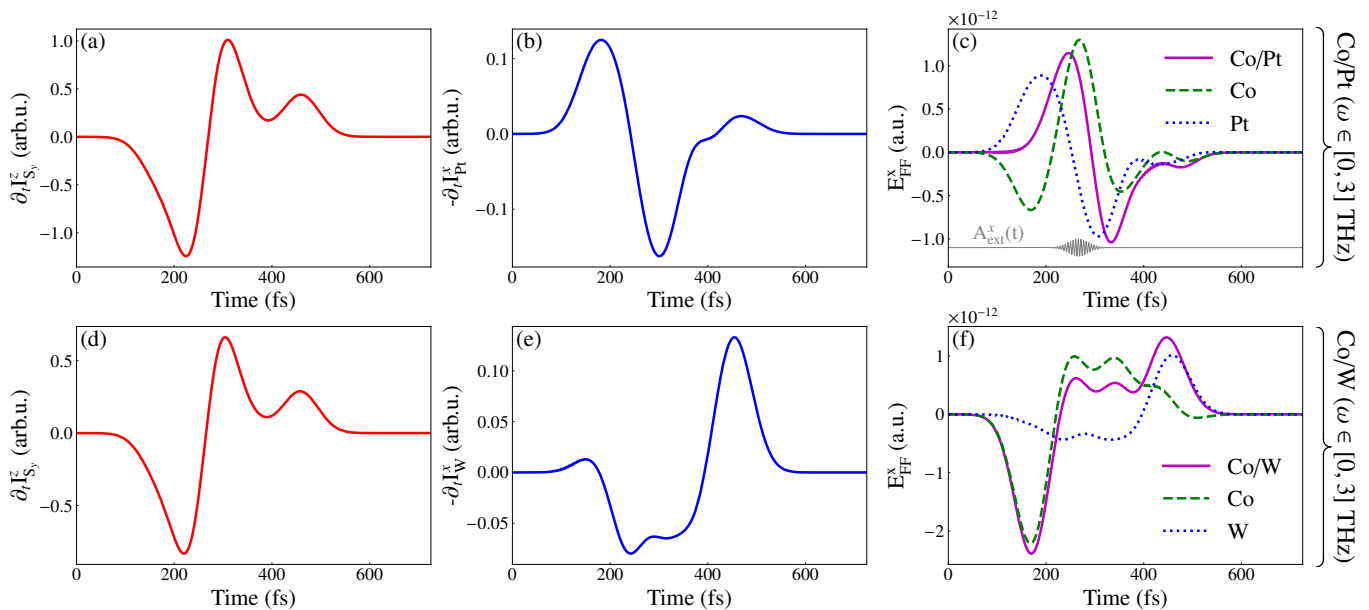


FIG. 3. Time dependence of time derivative of: (a) interlayer spin current $I_{S_y}^z$ in Co/Pt bilayer; and (b) charge current flowing within Pt layer of such bilayer. Panel (c) shows the x -component of electric field of THz radiation emitted by [time derivative via Eq. (4)] charge currents within Co (green) or Pt [blue, as it originates from current in panel (b)] layers, as well their sum as total radiation from Co/Pt bilayer. Panels (d)–(f) are counterparts of panels (a)–(c), but for Co/W bilayer. All six panels are obtained by using Fourier components within $\omega \in [0, 3]$ THz range to reconstruct the respective real time signals. Gray curve in (c) depicts vector potential $A_{\text{ext}}^x(t)$ of fsLP in Eq. (5).

Fig. 2 replaces the need for phenomenological “spin voltage” as its driving mechanism [2, 4, 14]. Findings of Fig. 2 also provide microscopic justification for previously conjectured “ dM/dt mechanism” [4, 36, 37] from the fitting of experimental data and thereby motivated phenomenological theories [17]. Once demagnetization sets in, the amplitude of generated spin current is primarily determined by the speed of demagnetization, which is larger in Co/Pt than in Co/W [compare values around $\simeq 50$ fs in Fig. 2(a) vs. Fig. 2(b)] due to difference in SOC-proximity effect [38, 39]. Via such proximity effect, Pt or W layer can significantly modify [38] properties of Co layer, of nanoscale thickness in experiments, as also confirmed in ultrafast demagnetization experiments [40]. Experiments also find [41] that interlayer spin current can affect demagnetization in self-consistent fashion—demagnetization acts as a primary nonequilibrium drive of spin current in THz frequency range in Fig. 2, which in turn further speeds up [41] demagnetization as spin current carries away angular momentum from Co into good spin sinks [30] like Pt or W.

Note that $I_{S_y}^z \neq 0$ being nonzero in the early stage ($t < 25$ fs), during which $\partial_t M^y \simeq 0$ [Fig. 2], can be explained by the presence [42] of a second nonequilibrium drive (the fsLP) that is initially the only one. In addition, since electrons respond instantaneously to fsLP, the start of oscillations of red curves in Fig. 2 signals the beginning of fsLP (see movies accompanying Ref. [43] for

further illustration of such generic feature of fsLP-solids interaction).

We next examine if a causal connection between interlayer spin current [Eq. (2)] and charge current

$$I_{\text{NM}}^x(t) = \int_{\text{NM}} d^3 r j^x(\mathbf{r}, t), \quad (3)$$

flowing within NM=Pt or NM=W layer, along the x -axis in Fig. 1 in accord with ISHE [9], also produces one-to-one relation [Eq. 1] between spin and charge currents. Here $j^x(\mathbf{r}, t)$ is the x -component of the vector of charge current density. Such relation is virtually always (for exceptions, see Ref. [21]) assumed [1–5] when interpreting experiments. Since EM radiation in the far-field region scanned experimentally is generated by the time-derivative of charge current [Eq. (4)], rather than by current itself as sometimes *incorrectly* assumed [1, 2, 4, 5], we plot in Fig. 3(a) time-derivative of spin current $\partial_t I_{S_y}^z$ in Co/Pt from Fig. 2(a) and compare it with time-derivative of charge current $\partial_t I_{\text{NM}}^x$ within Pt in Fig. 3(b). The same comparison is performed in Fig. 3(d) vs. Fig. 3(e) for Co/W bilayer. As spin and charge current profiles differ, we conclude that Eq. (1) is *not justified*, thereby supporting the same conclusion of experiments in Ref. [21].

Finally, we examine if charge current within the NM layer, generated by possibly multiple spin-to-charge conversion processes [21, 44, 45] of incoming interlayer spin current in Fig. 2, is the sole contributor to outgoing THz

radiation, as virtually always assumed [1–5] when interpreting experiments. We note that despite being one of the main observables in experiments, both for single FM layer [46] and FM/NM bilayers [1–5], EM radiation has been scarcely calculated. A microscopic, as well as first principles, route for such an analysis has been formulated very recently as TDDFT+Jefimenko approach [28]. In it, charge current densities computed from TDDFT are plugged into the Jefimenko formula [47] for the electric field of EM radiation in the far-field region [48], as given by

$$\mathbf{E}_{\text{FF}}(\mathbf{r}, t) = \frac{1}{4\pi\epsilon_0} \int_{\substack{\text{FM, NM,} \\ \text{or FM/NM}}} d^3r' \left(\mathbf{R} \frac{\partial_t \mathbf{j}_{\text{ret}} \cdot \mathbf{R}}{c^2 R^3} - \frac{\partial_t \mathbf{j}_{\text{ret}}}{c^2 R} \right). \quad (4)$$

Here charge current density $\mathbf{j}_{\text{ret}}(\mathbf{r}, t) = \mathbf{j}(\mathbf{r}, t - R/c)$ is evaluated at the retarded time $t - R/c$; c is the velocity of light; $\mathbf{R} = \mathbf{r} - \mathbf{r}'$ is the vector from source at a point \mathbf{r}' within FM/NM bilayer to the observation point \mathbf{r} ; and we also use shorthand notation $R = |\mathbf{R}|$. The observation point is chosen as $\mathbf{r} = 10000a_B\mathbf{e}_z$, where a_B is the Bohr radius, and the origin of the coordinate system is in the lower left corner of Co layer [Fig. 1]. The far-field region is defined as the region where EM radiation decays as $\sim 1/R$, which isolates [48] two terms from the full Jefimenko formula [47, 49] for electric field at arbitrary distance. Note that full Jefimenko formulas for electric and magnetic field of EM radiation can be viewed [49] as the proper time-dependent and time-retarded [via usage of $\mathbf{j}_{\text{ret}}(\mathbf{r}, t)$] generalizations of the Coulomb and Biot-Savart laws, respectively. They are an integral solution of the Maxwell equations in the following approximations: fields vanish at infinity; their sources are confined to a finite region of space; and self-consistent effects, such as emitted EM radiation exerting backaction [50, 51] onto the source, can be neglected.

Figure 3(c) shows that the real-time signal of THz radiation contains contributions from charge currents within *both* Pt and Co layers, which can be spatially resolved by limits of integration in Eq. (4). The latter current has been predicted very recently by Refs. [28, 35] as an additional consequence of $\partial_t M^y(t)$ that acts as a nonequilibrium drive for electrons. Compared to the time profile of fsLP, the initial nonequilibrium drive, the time dependence of $\partial_t M^y(t)$ has different spectral content [27] and always pumps *both* spin [Fig. 2] and charge currents. This feature can be contrasted to current pumping by precessing magnetization driven by low frequency EM radiation, which typically generates only spin current [30, 34]. The two contributions do not simply enhance each other due to their different phase—in fact, the contribution from Pt slightly reduces [Fig. 3(f)] the signal dominated by charge current flowing within Co layer.

When switching from Co/Pt to Co/W bilayer, the contribution to THz signal from spin-to-charge converted

current flowing within W layer is, surprisingly, insignificant [blue dotted line in Fig. 3(f)] when compared to the contribution from charge current flowing within Co layer [green dashed line in Fig. 3(f)]. The same information, as charge current and THz signal are related via Jefimenko Eq. (4), is obtained by comparing Fig. 3(e) vs. Fig. 3(b) where $\partial_t I_{\text{W}}^x$ in the former is an order of magnitude smaller than $\partial_t I_{\text{Pt}}^x$ in the latter. Thus, this finding provides quite a different explanation for the observed [2] change of sign of THz signal when switching from NM=Pt to NM=W layer, which is usually attributed [2] to the opposite sign of θ_{SH} of Pt and W that subsequently inverts the charge current within NM layer assuming Eq. (1) holds true.

The fact that the charge current within the W layer is small, thereby having very little effect on the total THz signal in Fig. 3(f), highlights the intricacies of both spin transport across FM/NM interfaces and ultrafast dynamics of electrons in general. Regarding former, naïve assumption that any NM layer with strong SOC and large θ_{SH} , such as W, automatically performs efficient spin-to-charge conversion in accord with Eq. (1) is *not warranted* as spin current could be diminished at the interface due to SOC [52–56] combined with possible lattice mismatch [54] or interfacial disorder [54], as well as due to magnetic moment reduction [57] on the FM side for 3d FM layers whose states hybridize strongly with 5d states of heavy metals. Regarding latter and unrelated to spin transport, usage of transition metals as NM layers makes possible localization [58] of excited electrons onto the outer unfilled *d*-orbitals of W as a signature of transition from initially independent into collective electron dynamics that has been observed in recent attosecond transient absorption spectroscopy experiments [59].

Models and Methods.—The TDDFT calculations were performed via extended-by-us [28] ELK package [23, 24]. The thicknesses of Co is three and of Pt or W is four monolayers (MLs) along [100] crystallographic direction. In the TDDFT formalism, the time-dependent Kohn-Sham (KS) equation for Pauli spinors of KS orbitals is given by (using $\hbar = 1$)

$$i \frac{\partial \psi_j(\mathbf{r}, t)}{\partial t} = \left[\frac{1}{2m_e} \left(-i\nabla + \frac{1}{c} \mathbf{A}_{\text{ext}}(t) \right)^2 + v_s(\mathbf{r}, t) + \frac{1}{2c} \boldsymbol{\sigma} \cdot \mathbf{B}_s(\mathbf{r}, t) + \frac{1}{4c^2} \boldsymbol{\sigma} \cdot (\nabla v_s(\mathbf{r}, t) \times -i\nabla) \right] \psi_j(\mathbf{r}, t), \quad (5)$$

where m_e is the electron mass; $\mathbf{A}_{\text{ext}}(t)$ is the vector potential of the applied fsLP; $v_s(\mathbf{r}, t) = v_{\text{ext}}(\mathbf{r}, t) + v_{\text{H}}(\mathbf{r}, t) + v_{\text{XC}}(\mathbf{r}, t)$ is the effective KS potential, as the sum of the external potential v_{ext} provided by the nuclei (treated as point particles), the Hartree potential v_{H} and exchange (XC) potential v_{XC} ; $\mathbf{B}_s(\mathbf{r}, t) = \mathbf{B}_{\text{ext}}(t) + \mathbf{B}_{\text{XC}}(t)$ is the KS magnetic field with \mathbf{B}_{ext} being the external magnetic

field and \mathbf{B}_{XC} the XC magnetic field; $\boldsymbol{\sigma} = (\sigma_x, \sigma_y, \sigma_z)$ is the vector of the Pauli matrices; and the last term on the RHS describes SOC which necessitates usage of noncollinear XC functionals [60, 61] even when long-range noncollinearity of local magnetization does not play a significant role. The particle density of an interacting electronic system, as the fundamental quantity in (TD)DFT, is obtained from noninteracting KS electrons orbitals through $n(\mathbf{r}, t) = \sum_j \psi_j^\dagger(\mathbf{r}, t)\psi_j(\mathbf{r}, t)$. Similarly, magnetization density, as an additional fundamental quantity in noncollinear (TD)DFT, is obtained from $\mathbf{m}(\mathbf{r}, t) = \sum_j \psi_j^\dagger(\mathbf{r}, t)\boldsymbol{\sigma}\psi_j(\mathbf{r}, t)$, so that total magnetization is given by $\mathbf{M}(t) = \int d^3r \mathbf{m}(\mathbf{r}, t)$. We employ adiabatic local density approximation (ALDA) for XC functional [62] within full-potential linearized augmented plane-wave method as implemented in the ELK code [23, 24]. The ground state (GS) is also obtained from ELK using noncollinear static DFT calculations with LDA XC functional. The grid of \mathbf{k} vectors is chosen as 7×7 for both Co/Pt or Co/W. After obtaining the GS, the dynamics for TDDFT calculations is generated by applying a Gaussian fsLP with: central wavelength 800 nm; $\simeq 50$ fsLP duration; the peak intensity of 2.42 TW/cm²; and 22 mJ/cm² fluence. Since the wavelength of applied laser light is much larger than the supercell, we assume dipole approximation and disregard spatial dependence of the vector potential $\mathbf{A}_{\text{ext}}(t)$.

Conclusions and Outlook.—Using recently developed TDDFT+Jefimenko first-principles approach [28], we have independently and microscopically evaluated spin and charge currents in response to fsLP driving Co/Pt and Co/W bilayers to find [Fig. 3] that in both cases

$$I_{\text{NM}}^x(t) \neq \theta_{\text{SH}} I_{\text{S}_y}^z(t), \quad (6)$$

in the case of time-dependent transport at *ultrafast* time scales. This is in contrast to their equality via Eq. (1) that is virtually always assumed [1–5] when interpreting experiments, as well as used [5] to extract $I_{\text{S}_y}^z(t)$ time profile from measured THz signals. There are many reasons for Eq. (6) and the lack [Fig. 3] of direct relation [22] between time profiles of $I_{\text{S}_y}^z(t)$ and THz signal, also conjectured from recent experiments of Ref. [21] but indirectly, as spin current cannot be directly measured in general, and measuring ultrafast charge current is outside the capabilities of presently available electronics. For example, multiple spin-to-charge conversion processes—such as, at FM/NM interface or within NM bulk [44]; spin memory loss [52–56]; reduced spin transmission [57] across FM/NM interface; and localization [58, 59] of initially free excited electrons onto outer unfilled d -orbitals of transition metals used as NM layer—can easily disrupt naively conjectured one-to-one relation [Eq. 1] between interlayer spin current along the z -axis and charge current along the x -axis within NM layer in Fig. 1.

Our first-principles analysis also reveals that $I_{\text{S}_y}^z(t) \propto$

$\partial_t M^y(t)$ [Fig. 2], thereby explaining how the origin of interlayer spin current is its pumping by time dependence of $M^y(t)$. This akin to standard [30, 34] spin pumping by precessing magnetization $\mathbf{M}(t)$ of fixed length. However, in demagnetization phenomenon [6–8] $\mathbf{M}(t)$ is shrinking in length without [18, 28] rotating because of FM layer absorbing fsLP, rather than rotating as a vector of fixed length when microwaves are absorbed in standard spin pumping setup [31]. Thus, the findings of Fig. 2 displace the need for phenomenological “spin voltage” as the driving mechanism [2, 4, 14] of interlayer spin current. Unlike conventional pure spin current pumping by precessing magnetization [30], where accompanying charge current is absent (unless additional ingredients are included [34, 63–65]), demagnetization dynamics is *always accompanied* by charge current pumping, as predicted very recently [28, 35]. Furthermore, thus pumped charge current $I_{\text{FM}}^x(t)$ flowing within the FM layer can dominate the real-time THz signal, as revealed by Figs. 3(c) and 3(f). Due to the phase difference in contributions [via Jefimenko Eq. (4)] to EM radiation from charge current densities $j_{\text{Co}}^x(\mathbf{r}, t)$ and $j_{\text{Pt}}^x(\mathbf{r}, t)$, we find a delay in total THz signal in the case of Co/Pt bilayer [see Fig. 3(c)], which is otherwise interpreted by variety of plausible notions [2]. In the case of Co/W bilayer, we find a surprisingly little effect [Fig. 3(f)] of $j_{\text{W}}^x(\mathbf{r}, t)$ on the total THz signal, which has previously been considered as the sole source of such signal [2]. This feature arises due to localization [59] of excited electrons onto the outer unfilled d -orbitals of W as the consequence of general properties of ultrafast electron dynamics [58, 59], thereby making standardly assumed and derived from intuition based on linear-response steady-state transport phenomena [20, 66] spin-to-charge conversion [1–5] via ISHE in W largely *inoperative* [Fig. 3(e)]. It also furnishes an extreme example of inequality in Eq. (6).

This research was supported by the US National Science Foundation (NSF) through the University of Delaware Materials Research Science and Engineering Center, DMR-2011824. The supercomputing time was provided by DARWIN (Delaware Advanced Research Workforce and Innovation Network), which is supported by NSF Grant No. MRI-1919839.

* bnikolic@udel.edu

- [1] T. Seifert, S. Jaiswal, U. Martens, J. Hannegan, L. Braun, P. Maldonado, F. Freimuth, A. Kronenberg, J. Henrizi, I. Radu, *et al.*, Efficient metallic spintronic emitters of ultrabroadband terahertz radiation, *Nat. Photonics* **10**, 483 (2016).
- [2] T. S. Seifert, D. Go, H. Hayashi, R. Rouzgar, F. Freimuth, K. Ando, Y. Mokrousov, and T. Kampfrath, Time-domain observation of ballistic orbital-angular-momentum currents with giant relaxation length in tung-

- sten, *Nat. Nanotechnol.* **18**, 1132 (2023).
- [3] Y. Wu, M. Elyasi, X. Qiu, M. Chen, Y. Liu, L. Ke, and H. Yang, High-performance THz emitters based on ferromagnetic/nonmagnetic heterostructures, *Adv. Mater.* **29**, 1603031 (2017).
 - [4] R. Rouzegar, L. Brandt, L. c. v. Nádvořník, D. A. Reiss, A. L. Chekhov, O. Gueckstock, C. In, M. Wolf, T. S. Seifert, P. W. Brouwer, *et al.*, Laser-induced terahertz spin transport in magnetic nanostructures arises from the same force as ultrafast demagnetization, *Phys. Rev. B* **106**, 144427 (2022).
 - [5] J. Jechumtál, R. Rouzegar, O. Gueckstock, C. Denker, W. Hoppe, Q. Remy, T. S. Seifert, P. Kubaščík, G. Woltersdorf, P. W. Brouwer, M. Münzenberg, T. Kampfrath, and L. Nádvořník, Accessing ultrafast spin-transport dynamics in copper using broadband terahertz spectroscopy, *Phys. Rev. Lett.* **132**, 226703 (2024).
 - [6] E. Beaurepaire, J.-C. Merle, A. Daunois, and J.-Y. Bigot, Ultrafast spin dynamics in ferromagnetic nickel, *Phys. Rev. Lett.* **76**, 4250 (1996).
 - [7] A. Kirilyuk, A. V. Kimel, and T. Rasing, Ultrafast optical manipulation of magnetic order, *Rev. Mod. Phys.* **82**, 2731 (2010).
 - [8] P. Scheid, Q. Remy, S. Lebègue, G. Malinowski, and S. Mangin, Light induced ultrafast magnetization dynamics in metallic compounds, *J. Magn. Magn. Mater.* **560**, 169596 (2022).
 - [9] E. Saitoh, M. Ueda, H. Miyajima, and G. Tatara, Conversion of spin current into charge current at room temperature: Inverse spin-Hall effect, *Appl. Phys. Lett.* **88**, 182509 (2006).
 - [10] M. B. Jungfleisch, Q. Zhang, W. Zhang, J. E. Pearson, R. D. Schaller, H. Wen, and A. Hoffmann, Control of terahertz emission by ultrafast spin-charge current conversion at Rashba interfaces, *Phys. Rev. Lett.* **120**, 207207 (2018).
 - [11] O. Gueckstock, L. Nádvořník, M. Gradhand, T. S. Seifert, G. Bierhance, R. Rouzegar, M. Wolf, M. Vafaei, J. Cramer, M. A. Syskaki, *et al.*, Terahertz spin-to-charge conversion by interfacial skew scattering in metallic bilayers, *Adv. Mater.* **33**, 2006281 (2021).
 - [12] Y. Wang, W. Li, H. Cheng, Z. Liu, Z. Cui, J. Huang, B. Xiong, J. Yang, H. Huang, J. Wang, *et al.*, Enhancement of spintronic terahertz emission enabled by increasing Hall angle and interfacial skew scattering, *Commun. Phys.* **6**, 280 (2023).
 - [13] W.-T. Lu, Y. Zhao, M. Battiato, Y. Wu, and Z. Yuan, Interface reflectivity of a superdiffusive spin current in ultrafast demagnetization and terahertz emission, *Phys. Rev. B* **101**, 014435 (2020).
 - [14] K. Bühlmann, G. Saerens, A. Vaterlaus, and Y. Acremann, Detection of femtosecond spin voltage pulses in a thin iron film, *Struct. Dyn.* **7**, 065101 (2020).
 - [15] M. Battiato, K. Carva, and P. M. Oppeneer, Superdiffusive spin transport as a mechanism of ultrafast demagnetization, *Phys. Rev. Lett.* **105**, 027203 (2010).
 - [16] D. M. Nenno, R. Binder, and H. C. Schneider, Simulation of hot-carrier dynamics and terahertz emission in laser-excited metallic bilayers, *Phys. Rev. Appl.* **11**, 054083 (2019).
 - [17] M. Beens, R. A. Duine, and B. Koopmans, Modeling ultrafast demagnetization and spin transport: The interplay of spin-polarized electrons and thermal magnons, *Phys. Rev. B* **105**, 144420 (2022).
 - [18] K. Krieger, J. K. Dewhurst, P. Elliott, S. Sharma, and E. K. U. Gross, Laser-induced demagnetization at ultra-short time scales: Predictions of TDDFT, *J. Chem. Theory Comput.* **11**, 4870 (2015).
 - [19] G. P. Zhang and W. Hübner, Laser-induced ultrafast demagnetization in ferromagnetic metals, *Phys. Rev. Lett.* **85**, 3025 (2000).
 - [20] J. Sinova, S. O. Valenzuela, J. Wunderlich, C. H. Back, and T. Jungwirth, Spin hall effects, *Rev. Mod. Phys.* **87**, 1213 (2015).
 - [21] J. Gorchon, S. Mangin, M. Hehn, and G. Malinowski, Is terahertz emission a good probe of the spin current attenuation length?, *Appl. Phys. Lett.* **121**, 012402 (2022).
 - [22] G. Schmidt, B. Das-Mohapatra, and E. T. Papaioannou, Charge dynamics in spintronic terahertz emitters, *Phys. Rev. Appl.* **19**, L041001 (2023).
 - [23] J. K. Dewhurst, K. Krieger, S. Sharma, and E. K. U. Gross, An efficient algorithm for time propagation as applied to linearized augmented plane wave method, *Comput. Phys. Commun.* **209**, 92 (2016).
 - [24] The Elk Code, <http://elk.sourceforge.net/>.
 - [25] Z. Chen and L.-W. Wang, Role of initial magnetic disorder: A time-dependent *ab initio* study of ultrafast demagnetization mechanisms, *Sci. Adv.* **5**, eaau800 (2019).
 - [26] C. Pellegrini, S. Sharma, J. K. Dewhurst, and A. Sanna, *Ab initio* study of ultrafast demagnetization of elementary ferromagnets by terahertz versus optical pulses, *Phys. Rev. B* **105**, 134425 (2022).
 - [27] M. S. Mrudul and P. M. Oppeneer, *Ab initio* investigation of laser-induced ultrafast demagnetization of $L1_0$ FePt: Intensity dependence and importance of electron coherence, *Phys. Rev. B* **109**, 144418 (2024).
 - [28] A. Kefayati and B. K. Nikolić, Origins of electromagnetic radiation from spintronic terahertz emitters: A time-dependent density functional theory plus Jefimenko equations approach, *Phys. Rev. Lett.* **133**, 136704 (2024).
 - [29] N. Tancogne-Dejean, F. G. Eich, and A. Rubio, Effect of spin-orbit coupling on the high harmonics from the topological dirac semimetal Na_3Bi , *Npj Comput. Mater.* **8**, 145 (2022).
 - [30] Y. Tserkovnyak, A. Brataas, G. E. Bauer, and B. I. Halperin, Nonlocal magnetization dynamics in ferromagnetic heterostructures, *Rev. Mod. Phys.* **77**, 1375 (2005).
 - [31] K. Ando, Dynamical generation of spin currents, *Semiconductor Science and Technology* **29**, 043002 (2014).
 - [32] R. Citro and M. Aidelsburger, Thouless pumping and topology, *Nat. Rev. Phys.* **5**, 87 (2023).
 - [33] P. W. Brouwer, Scattering approach to parametric pumping, *Phys. Rev. B* **58**, R10135 (1998).
 - [34] J. Varela-Manjarres and B. K. Nikolić, High-harmonic generation in spin and charge current pumping at ferromagnetic or antiferromagnetic resonance in the presence of spin-orbit coupling, *J. Phys.: Mater.* **6**, 045001 (2023).
 - [35] J. Varela-Manjarres, A. Kefayati, M. B. Jungfleisch, J. Q. Xiao, and B. K. Nikolić, Charge and spin current pumping by ultrafast demagnetization dynamics, *Phys. Rev. B* **110**, L060410 (2024).
 - [36] G.-M. Choi, B.-C. Min, K.-J. Lee, and D. G. Cahill, Spin current generated by thermally driven ultrafast demagnetization, *Nat. Commun.* **5**, 4334 (2014).
 - [37] T. Lichtenberg, M. Beens, M. H. Jansen, B. Koopmans, and R. A. Duine, Probing optically induced spin currents using terahertz spin waves in noncollinear magnetic bilayers, *Phys. Rev. B* **105**, 144416 (2022).

- [38] J. M. Marmolejo-Tejada, K. Dolui, P. Lazić, P.-H. Chang, S. Smidstrup, D. Stradi, K. Stokbro, and B. K. Nikolić, Proximity band structure and spin textures on both sides of topological-insulator/ferromagnetic-metal interface and their charge transport probes, *Nano Lett.* **17**, 5626 (2017).
- [39] I. Žutić, A. Matos-Abiague, B. Scharf, H. Dery, and K. Belashchenko, Proximitized materials, *Materials Today* **22**, 85 (2019).
- [40] K. Kuiper, T. Roth, A. Schellekens, O. Schmitt, B. Koopmans, M. Cinchetti, and M. Aeschlimann, Spin-orbit enhanced demagnetization rate in Co/Pt-multilayers, *Appl. Phys. Lett.* **105**, 1 (2014).
- [41] G. Malinowski, F. D. Longa, J. H. H. Rietjens, P. V. Paluskar, R. Huijink, H. J. M. Swagten, and B. Koopmans, Control of speed and efficiency of ultrafast demagnetization by direct transfer of spin angular momentum, *Nat. Phys.* **4**, 855 (2008).
- [42] A. Suresh and B. K. Nikolić, Quantum classical approach to spin and charge pumping and the ensuing radiation in terahertz spintronics: Example of the ultrafast light-driven Weyl antiferromagnet Mn_3Sn , *Phys. Rev. B* **107**, 174421 (2023).
- [43] U. Bajpai, B. S. Popescu, P. Plecháč, B. K. Nikolić, L. E. F. F. Torres, H. Ishizuka, and N. Nagaosa, Spatiotemporal dynamics of shift current quantum pumping by femtosecond light pulse, *J. Phys.: Mater.* **2**, 025004 (2019).
- [44] F. Mahfouzi, N. Nagaosa, and B. K. Nikolić, Spin-to-charge conversion in lateral and vertical topological-insulator/ferromagnet heterostructures with microwave-driven precessing magnetization, *Phys. Rev. B* **90**, 115432 (2014).
- [45] P. Agarwal, Y. Yang, R. Medwal, H. Asada, Y. Fukuma, M. Battiato, and R. Singh, Secondary spin current driven efficient THz spintronic emitters, *Adv. Opt. Mater.* **11**, 2301027 (2023).
- [46] E. Beaurepaire, G. M. Turner, S. M. Harrel, M. C. Beard, J.-Y. Bigot, and C. A. Schmuttenmaer, Coherent terahertz emission from ferromagnetic films excited by femtosecond laser pulses, *Appl. Phys. Lett.* **84**, 3465 (2004).
- [47] O. D. Jefimenko, *Electricity and Magnetism* (Appleton Century-Crofts, New York, 1966).
- [48] K. T. McDonald, The relation between expressions for time-dependent electromagnetic fields given by Jefimenko and by Panofsky and Phillips, *Am. J. Phys.* **65**, 1074 (1997).
- [49] D. J. Griffiths and M. A. Heald, Time-dependent generalizations of the Biot–Savart and Coulomb laws, *Am. J. Phys.* **59**, 111 (1991).
- [50] N. Tancogne-Dejean, M. J. T. Oliveira, X. Andrade, H. Appel, C. H. Borca, G. L. Breton, F. Buchholz, A. Castro, S. Corni, A. A. Correa, *et al.*, Octopus, a computational framework for exploring light-driven phenomena and quantum dynamics in extended and finite systems, *J. Chem. Phys.* **152**, 124119 (2020).
- [51] T. M. Philip and M. J. Gilbert, Theory of AC quantum transport with fully electrodynamic coupling, *J. Comput. Electron.* **17**, 934 (2018).
- [52] K. D. Belashchenko, A. A. Kovalev, and M. van Schilfgaarde, Theory of spin loss at metallic interfaces, *Phys. Rev. Lett.* **117**, 207204 (2016).
- [53] K. Dolui and B. K. Nikolić, Spin-memory loss due to spin-orbit coupling at ferromagnet/heavy-metal interfaces: *Ab initio* spin-density matrix approach, *Phys. Rev. B* **96**, 220403(R) (2017).
- [54] K. Gupta, R. J. H. Wesselink, R. Liu, Z. Yuan, and P. J. Kelly, Disorder dependence of interface spin memory loss, *Phys. Rev. Lett.* **124**, 087702 (2020).
- [55] V. P. Amin and M. D. Stiles, Spin transport at interfaces with spin-orbit coupling: Formalism, *Phys. Rev. B* **94**, 104419 (2016).
- [56] V. P. Amin and M. D. Stiles, Spin transport at interfaces with spin-orbit coupling: Phenomenology, *Phys. Rev. B* **94**, 104420 (2016).
- [57] M. A. Wahada, E. Şaşıoğlu, W. Hoppe, X. Zhou, H. Deniz, R. Rouzegar, T. Kampfrath, I. Mertig, S. S. P. Parkin, and G. Woltersdorf, Atomic scale control of spin current transmission at interfaces, *Nano Lett.* **22**, 3539 (2022).
- [58] M. Volkov, S. A. Sato, F. Schlaepfer, L. Kasmí, N. Hartmann, M. Lucchini, L. Gallmann, A. Rubio, and U. Keller, Attosecond screening dynamics mediated by electron localization in transition metals, *Nat. Phys.* **15**, 1145 (2019).
- [59] E. W. de Vos, S. Neb, A. Niedermayr, F. Burri, M. Hollm, L. Gallmann, and U. Keller, Ultrafast transition from state-blocking dynamics to electron localization in transition metal β -tungsten, *Phys. Rev. Lett.* **131**, 226901 (2023).
- [60] F. G. Eich and E. K. U. Gross, Transverse spin-gradient functional for noncollinear spin-density-functional theory, *Phys. Rev. Lett.* **111**, 156401 (2013).
- [61] F. Egidi, S. Sun, J. J. Goings, G. Scalmani, M. J. Frisch, and X. Li, Two-component noncollinear time-dependent spin density functional theory for excited state calculations, *J. Chem. Theory Comput.* **13**, 2591 (2017).
- [62] L. Lacombe and N. T. Maitra, Non-adiabatic approximations in time-dependent density functional theory: progress and prospects, *npj Comput. Mater.* **9**, 124 (2023).
- [63] S.-H. Chen, C.-R. Chang, J. Q. Xiao, and B. K. Nikolić, Spin and charge pumping in magnetic tunnel junctions with precessing magnetization: A nonequilibrium green function approach, *Phys. Rev. B* **79**, 054424 (2009).
- [64] K. M. D. Hals, A. Brataas, and Y. Tserkovnyak, Scattering theory of charge-current induced magnetization dynamics, *EPL (Europhysics Letters)* **90**, 47002 (2010).
- [65] C. Ciccarelli, K. M. D. Hals, A. Irvine, V. Novak, Y. Tserkovnyak, H. Kurebayashi, A. Brataas, and A. Ferguson, Magnonic charge pumping via spin-orbit coupling, *Nat. Nanotechnol.* **10**, 50 (2014).
- [66] D. Van Tuan, J. M. Marmolejo-Tejada, X. Waintal, B. K. Nikolić, S. O. Valenzuela, and S. Roche, Spin hall effect and origins of nonlocal resistance in adatom-decorated graphene, *Phys. Rev. Lett.* **117**, 176602 (2016).